Catalysis Today 163 (2011) 20–26

Contents lists available at ScienceDirect

Catalysis Today

journal homepage: www.elsevier.com/locate/cattod

Stability of metal nanoparticles formed during reduction of alumina supported nickel and cobalt catalysts

Bas M. Vogelaar [a,*], A. Dick van Langeveld [a], Patricia J. Kooyman [a], C. Martin Lok [b,1], Raimond L.C. Bonné [c,1], Jacob A. Moulijn [a]

[a] Delft University of Technology, Faculty of Applied Sciences, Julianalaan 136, 2628 BL Delft, The Netherlands
[b] Johnson Matthey Technology Centre Chilton, P.O. Box 1, Belasis Avenue, Billingham TS23 1LB, United Kingdom
[c] Johnson Matthey Chemicals GmbH, Wardstrasse 17, D46446 Emmerich am Rhein, Germany

ARTICLE INFO

Article history:
Available online 18 January 2010

Keywords:
Nickel
Cobalt
Temperature programmed reduction
Sintering
Morphology
Electron microscopy

ABSTRACT

The formation of nickel and cobalt nanoparticles in hydrogenation catalysts and their stability against sintering during the reduction of the oxidic precursors were investigated. The morphology of the catalysts was manipulated by varying the reduction conditions. The catalysts were characterized using temperature programmed reduction (TPR), hydrogen chemisorption, X-ray photoelectron spectroscopy (XPS) and high-resolution transmission electron microscopy (HREM). The transformation of the oxidic precursor into the active phase was monitored using *quasi in situ* HREM, which proved to be an excellent technique to visualize the formation of metal nanoparticles. For the nickel catalyst the reduction temperature plays a crucial role, whereas time is more critical for the cobalt catalyst. The sintering rate of cobalt is considerably lower than that of nickel during reduction. It is concluded that the activation energy for sintering is significantly higher for nickel than for cobalt. A model is proposed which depicts the structure of both types of catalysts in their oxidic and reduced state. TPR and XPS results indicate that the passivated catalysts contain approximately two oxygen atoms per surface Ni or Co atom.

1. Introduction

Most hydrogenation processes in chemical industry and food processing make use of nickel and cobalt catalysts because of their high performance and low cost. Such catalysts are subject of ongoing scientific studies [1–5]. Continuous improvement of analysis methods made it possible to obtain detailed information about the structure of these active materials and its effect on the catalytic activity. This has resulted in the development of hydrogenation catalysts, containing nano-sized nickel and cobalt particles with a high metal loading, a high specific metal surface area and a high reducibility [6].

The precursors are usually nickel and cobalt oxides supported on alumina. Nickel oxide-loaded catalysts have been characterized in earlier publications [6–8], and it was concluded that in the oxidic state Ni cations are present in highly dispersed NiO_x rafts with predominantly the (1 1 1) plane exposed to the gas phase [7]. At low loading (<4.5 wt% Ni) mainly single NiO_x layers are present whereas at higher loading two or three NiO_x layers are stacked. The stoichiometry of the surface phase was measured using TPR, and for x values between 1.2 and 1.5 were found, indicating an excess of oxygen at the surface [6]. Supported cobalt oxides with a high loading are usually found to be bidisperse systems [9–11]. At least two phases can be distinguished: bulk species of Co_3O_4 with a relatively large particle size and a highly dispersed cobalt species with a strong metal–support interaction [12].

The purpose of this work is to elucidate the formation mechanism of nickel and cobalt nanoparticles during the reduction of the oxidic precursors and to characterize their morphology. A second objective of this research is the assessment of the stability of these particles against sintering under prolonged treatment in hydrogen at high temperature during reduction. Both aims are important to define the optimal reduction conditions for the given catalytic system. The approach taken was to vary the reduction temperature and time, resulting in catalysts with different dispersion and morphology. The catalysts were characterized by temperature programmed reduction (TPR), hydrogen chemisorption, X-ray photoelectron spectroscopy (XPS) and high-resolution transmission electron microscopy (HREM). The formation of metal nanoparticles from the oxidic precursor was monitored using *quasi in situ* HREM.

* Corresponding author. Current address: Albemarle Catalysts BV, P.O. Box 37650, 1030 BE Amsterdam, The Netherlands. Tel.: +31 0 20 634 7648; fax: +31 0 20 634 7653.
E-mail address: Bas.Vogelaar@albemarle.com (B.M. Vogelaar).
[1] Authors are currently no longer affiliated with Johnson Matthey.

0920-5861/$ – see front matter © 2009 Elsevier B.V. All rights reserved.
doi:10.1016/j.cattod.2009.11.018

2. Experimental

2.1. Catalyst preparation

The catalyst precursors were supplied by Synetix; a commercial nickel oxide catalyst containing 15 wt% Ni supported on alumina (brand name HTC400) and a newly developed cobalt oxide catalyst containing 19 wt% Co supported on alumina. The oxidic precursors (1 mm extrudates) were crushed and sieved to a fraction of 90–210 μm. The precursors were reduced at different temperatures (723/873/1123 K) and duration (1/4 h) to obtain catalysts with varying dispersion and morphology, and subsequently they were passivated. Catalyst reduction was carried out in a fixed bed quartz reactor, using 2 g of catalyst, a hydrogen flow of 100 ml/min, and a heating rate of 10 K/min. After reduction the catalysts were cooled down in hydrogen and subsequently purged in nitrogen during 30 min. Then, the oxygen concentration was exponentially increased to 20 vol% during 120 min at room temperature, yielding the catalyst in its passivated state. Four passivated nickel catalysts and four passivated cobalt catalysts were prepared, labeled Ni or Co followed by the *reduction temperature* in K and the *reduction time* in hours.

2.2. Temperature programmed reduction

TPR analysis was performed in a custom-built setup equipped with a quartz fixed bed reactor which was loaded with 200 mg of catalyst diluted with 100 mg of SiC. The sample was heated according to a linear temperature program with a heating rate of 10 K/min up to 1273 K in a gas stream of 30 ml/min containing 7 vol% H_2 in argon. The amount of hydrogen consumed was recorded using a thermal conductivity detector (TCD). The recorded data was quantified using a calibration sample.

2.3. Hydrogen chemisorption

Hydrogen chemisorption was measured in a Quantachrome Autosorb-1-C analyzer. Approximately 200 mg of sample was placed in a glass fixed bed reactor. The passivated catalysts were dried overnight at 393 K and reduced at 523 K (heating rate 10 K/min) in a 50 ml/min hydrogen stream during 2 h. After reduction the reactor was evacuated at 723 K during 1 h to remove all chemisorbed H_2. After that the H_2 adsorption isotherm was recorded at 323 K. The sample was evacuated at the same temperature and the adsorption isotherm was measured again. This way the reversibly adsorbed hydrogen was excluded from the analysis. Both for Ni and Co a stoichiometry of one hydrogen atom per metal atom was assumed. The metal surface area and particle size were calculated using a density of 8.9 g/cc for Ni and Co, and a surface area of 6.49 and 6.62 $Å^2$ per Ni or Co atom, respectively.

2.4. XPS and HREM

XPS spectra of the reduced and passivated catalysts were acquired using a PerkinElmer PHI 5400 ESCA system equipped with a hemispherical analyzer. Mg Kα radiation was used for sample excitation. The binding energies were calibrated using the (Al 2*p*) line of the support at 74.2 eV as the internal reference. Baseline correction and satellite peak removal were performed using built in algorithms of the data acquisition software.

Transmission electron microscopy was performed using a Philips CM30T electron microscope with a LaB_6 filament at 300 kV as electron source. Samples were prepared by grinding the catalysts and suspending in ethanol. A few droplets of the suspension were applied on a carbon polymer microgrid supported on a copper grid and transferred to the microscope. In a separate series of experiments, the copper grid containing the oxidic catalyst was transferred to a glass reactor where the catalyst was reduced *in situ*. The copper grid was transferred back to the microscope and micrographs were recorded at exactly the same position in the catalyst sample as before reduction. The procedure was repeated using an oxygen treatment to obtain the micrographs of the reduced and passivated samples. This way detailed information could be obtained on the transformation of specific metal particles from the oxidic to the reduced and passivated state.

3. Results

3.1. TPR analyses

Fig. 1 shows the measured TPR patterns of the nickel catalysts. Three different species were identified which reduce in different temperature regions marked I, II and III in the figure. In the pattern of the oxidic precursor, two reduction peaks can be distinguished. In region I a small peak is observed around 550 K indicated in the figure by an arrow. In region II a large broad peak with its maximum at 750 K is observed which accounts for nearly all of the nickel present in the sample. In the patterns of the reduced and passivated samples this broad peak in region II has disappeared. Instead, in region I a large, sharp peak is observed around 525 K, of which the area under the peak declines with increasing reduction temperature and time. In the TPR pattern of the catalyst reduced at the lowest temperature, a broad feature is observed around 900 K in region III.

The oxidic precursor of the cobalt catalyst shows two complex reduction peaks (Fig. 2). Again a low temperature peak is found in region I around 600 K with a shoulder at the low temperature side. The other two features around 950 and 1050 K correspond to cobalt phases with a strong metal–support interaction (regions II

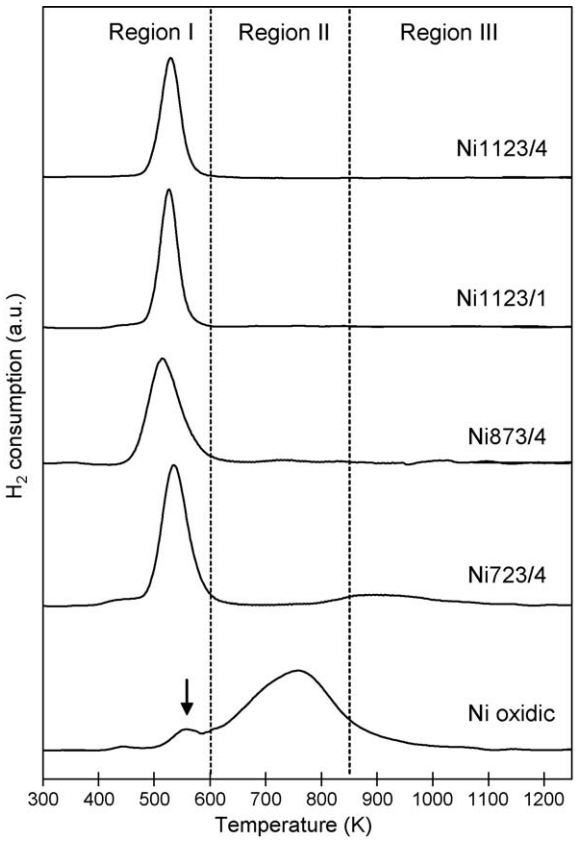

Fig. 1. Temperature programmed reduction patterns of the nickel catalysts.

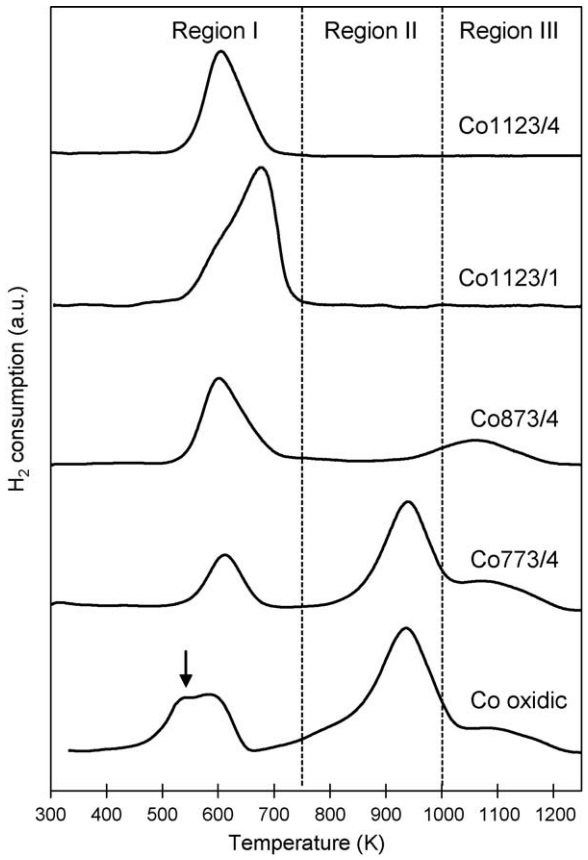

Fig. 2. Temperature programmed reduction patterns of the cobalt catalysts.

and III). After reduction at 773 K during 4 h, minor differences can be seen between the reduced sample and the oxidic precursor, only the low temperature shoulder in region I has disappeared (indicated by the arrow). After reduction at 873 K for 4 h, the peak at 950 K (region II) has disappeared, while the peak in region II has strongly increased. Following reduction at 1123 K during 1 h the peak in region III (around 1050 K) has disappeared and the catalyst is reduced completely in region I (around 650 K). The latter peak has a complex shape with a relatively steep descent at the high temperature side, however after reduction at 1123 K for 4 h a different peak shape is observed: the peak maximum is now shifted to a lower temperature (600 K), and tailing is present on the high temperature side.

By deconvoluting and integrating the peaks in the TPR patterns, individual contributions to the hydrogen consumption could be calculated. These values were normalized to the amount of metal in the samples and are summarized in Table 1. The reduction degree was calculated using the stoichiometry of the metal oxide phases on the catalysts as described in Section 4.

Table 1
Hydrogen uptake by TPR.

Catalyst	Hydrogen uptake (mol H_2/mol total Ni or Co)				Reduction degree[a] (%)
	Region I	Region II	Region III	Total	
Ni(ox)	0.17	1.1	0.15	1.42	–
Ni723/4	0.69	–	0.16	0.85	84
Ni873/4	0.65	–	–	0.65	100
Ni1123/1	0.48	–	–	0.48	100
Ni1123/4	0.45	–	–	0.45	100
Co(ox)	0.31	0.81	0.28	1.40	–
Co773/4	0.20	0.45	0.33	0.98	39
Co873/4	0.41	–	0.23	0.64	77
Co1123/1	0.76	–	–	0.76	100
Co1123/4	0.43	–	–	0.43	100

[a] Before passivation.

3.2. Hydrogen chemisorption data

Table 2 shows the results from the hydrogen chemisorption analyses. The data were normalized to the amount of reduced metal, as found by TPR. The nickel catalyst shows a high dispersion and a high metallic surface area that decreases with reduction temperature and time. For cobalt, the optimal conditions are 1123 K and 1 h. In spite of the higher loading the cobalt catalysts seem to have much lower metal surface areas than their nickel-based counterparts using hydrogen chemisorption. However, this was probably caused by an experimental error, as will be addressed in Section 4.

3.3. XPS results

Table 3 shows the peak areas of the baseline and satellite corrected XPS data. The (3*p*) bands of nickel and cobalt were deconvoluted into metallic and oxidic contributions using a peak fitting algorithm. The (2*p*) bands of nickel and cobalt exhibited large shake-up peaks and could not be deconvoluted. Using these data, the "oxidic fraction" could be calculated by dividing the metallic contribution by the total contribution. The ratio of the active metal signal (peak area), in this case (Ni 3*p*) or (Co 3*p*), to the aluminum (Al 2*p*) signal, is generally an indication for the dispersion [13]. This is valid when one surface phase is present with a homogeneous size distribution. The oxidic fraction and metal/aluminum ratios are included in the table. For both types of catalysts the metal/aluminum ratio gradually decreases with increasing reduction temperature and time. Only the cobalt sample with the lowest reduction temperature (773 K) does not follow the trend, caused by the fact that only a small portion of the cobalt has been reduced in that case.

Table 2
Hydrogen chemisorption results.

Catalyst	Monolayer uptake[a] (10^{-3} mol H_2/mol Ni^0 or Co^0)	Surface area (m^2/g catalyst)	Surface area[a] (m^2/g Ni^0 or Co^0)	Dispersion[a] (%)	Cluster size[a] (nm)
Ni723/4	107	18.0	142	21	4.7
Ni873/4	95	19.1	127	19	5.3
Ni1123/1	49	9.9	66	10	10.2
Ni1123/4	51	10.3	69	10	9.8
Co773/4	13	1.4	19	2.7	35
Co873/4	17	3.4	23	3.5	29
Co1123/1	30	7.7	41	6.0	17
Co1123/4	17	4.3	23	3.3	30

[a] Corrected for reduction degree (TPR).

Table 3
Peak areas of XPS analyses.

Catalyst	Ni^0 (a.u.) Co^0 (a.u.)	Ni^{2+} (a.u.) Co^{2+} (a.u.)	Al^{3+} (a.u.)	Ni/Al Co/Al	Ni^{2+}/Ni Co^{2+}/Co
Ni723/4	3.60	1.01	9.5	0.49	0.22
Ni873/4	3.44	1.07	10.6	0.43	0.24
Ni1123/1	2.64	1.40	11.0	0.37	0.35
Ni1123/4	2.52	0.89	10.3	0.33	0.26
Co773/4	2.78	0.90	10.1	0.36	0.25
Co873/4	1.76	0.93	10.1	0.27	0.34
Co1123/1	2.60	0.79	10.8	0.31	0.23
Co1123/4	1.32	0.65	12.6	0.16	0.33

Table 4
Crystallite size estimations – comparison of techniques.

Catalyst[a]	Dispersion[b] (%)	Metal/ aluminum ratio by XPS	Average cluster size[b] (nm)	Cluster size range by HREM (nm)
Ni1123/1	10	0.37	10.2	5–12
Ni1123/4	10	0.33	9.8	5–12
Ni873/4	19	0.43	5.3	2–15
Ni723/4	21	0.49	4.7	3–6
Co773/4	2.7	0.36	35	2–20
Co1123/4	3.3	0.16	30	2–25
Co873/4	3.5	0.27	29	4–25
Co1123/1	6.0	0.31	17	5–12

[a] The catalysts are ranked by increasing dispersion.
[b] Measured by hydrogen chemisorption, see Section 4.2.

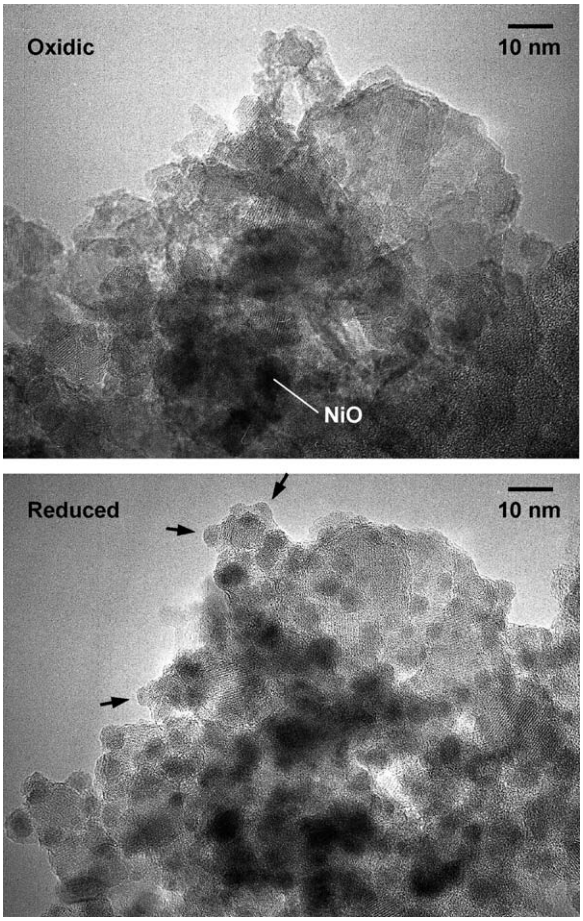

Fig. 3. HREM image of nickel catalyst before (oxidic) and after reduction at 723 K during 4 h.

3.4. HREM

In the HREM micrographs of the reduced and passivated catalysts nickel and cobalt crystallites of various sizes were identified (not shown). A rough estimate of the particle size range was made using four representative micrographs of each sample. Table 4 lists the results, together with the average cluster size obtained from the hydrogen chemisorption measurements. For the nickel catalysts the estimated values are in excellent agreement with the chemisorption data. For cobalt however, hydrogen chemisorption predicted larger particles than observed by HREM.

The *quasi in situ* method proved to be an excellent tool to study the transformation of the oxidic precursor into the reduced and passivated catalyst. Two examples are shown in Fig. 3 (the nickel catalyst) and Fig. 4 (the cobalt catalyst). Because the lattice spacings of NiO and Co_3O_4 are very similar to Al_2O_3 it is not easy to distinguish between these phases when they are highly dispersed. However, particles of NiO and Co_3O_4 could be identified for the oxidic precursors, as indicated in the figures. After reduction the formation of nickel and cobalt nanoparticles can clearly be observed. The crystallites at the edge of the sample are well

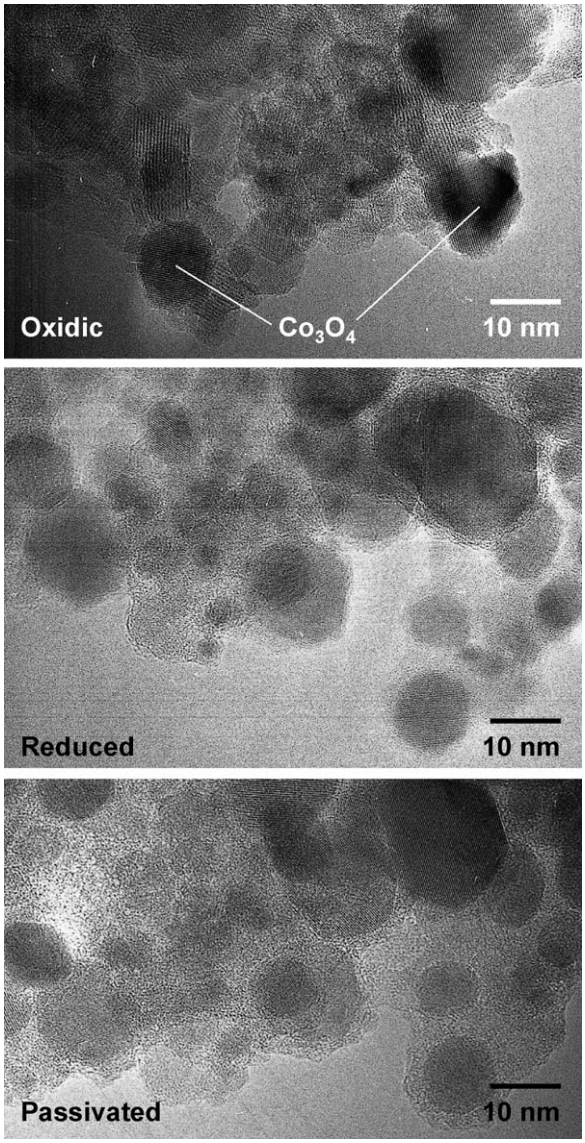

Fig. 4. HREM image of cobalt catalyst: before reduction (oxidic), after reduction at 873 K during 4 h, and after passivation.

visible. The nickel particles have their base plane perpendicular to the image plane (Fig. 3, marked by arrows) and appear to have a hemispherical shape. This was suggested earlier by Coenen and Lindsen [14] for Ni/SiO_2 catalysts. The cobalt particles appear to be spherical (Fig. 4). Upon passivation the observed particle size does not change, although this may be a visual artifact as the edge of the particles becomes more transparent due to oxidation of the outer edges [4].

4. Discussion

4.1. Identification of the surface phases on the catalyst

The TPR patterns indicate that the oxidic precursors of both types of catalysts contain three different nickel or cobalt containing phases, which reduce in specific temperature regions (Figs. 1 and 2; regions I, II and III). For nickel oxide on alumina hydrogen consumption in region I is attributed to the reduction of bulk NiO crystals [4,15]. These are present in low amounts at the outer surface of the support, as evidenced by HREM (Fig. 3). The TPR peak in region II is attributed to reduction of a highly dispersed nickel surface phase in strong interaction with the support, the NiO_x phase [6,15]. Other authors qualify this phase as a nickel surface spinel [3,16,17]. The feature in region III is attributed to nickel atoms which have migrated into the alumina support [18], which have a reduction temperature similar to bulk $NiAl_2O_4$ [19–21]. For cobalt oxide on alumina the peaks in region I evidence the two-step reduction of bulk Co_3O_4 [11,20,22–24]. This is apparently present in a substantial amount and was also identified in the HREM images (Fig. 4). This is not uncommon for supported cobalt catalysts with a high loading [11], and has been confirmed on γ-Al_2O_3 supported catalysts using XRD [5,25]. Such cobalt oxide particles could be identified in the HREM images (Fig. 4), in agreement with other TEM studies on cobalt catalyst systems [1,5]. Region II shows two peaks which are attributed to a highly dispersed cobalt oxide surface phase. This phase contains mainly Co^{2+} and possibly Co^{3+} ions [12,25–27], sometimes referred to as a cobalt surface spinel [24]. The peak in region III represents cobalt ions that have migrated into the alumina, which are very hard to reduce, like in bulk $CoAl_2O_4$ [12,20,21,23,24].

Using the above data, the stoichiometry of the highly dispersed nickel and cobalt oxide phases (region II) could be determined. The formation of hydrides (NiH and CoH) in this temperature region was ruled out because these compounds decompose at higher temperatures [17], which would be visible in the TPR pattern as a negative peak (release of hydrogen). It is therefore assumed that all hydrogen consumed is due to reaction with oxygen atoms in the sample. It was found that the NiO_x and CoO_x surface phases have equal stoichiometry with $x = 1.6$ indicating an excess of oxygen in these surface compounds. This value is close to the values reported for nickel by Hoffer et al. [6], and the observations of Okamoto et al. for cobalt on silica [10]. The presence of cobalt hydroxides was ruled out by Ji et al. using XPS [20], but Hoffer et al. seemed to positively identify a nickel hydroxide species using XPS [6]. Nickel has exclusively a +2 valence, as found by Shido et al. using EXAFS analysis on this type of catalyst [7]. This suggests that a substantial amount of chemisorbed zero-valent oxygen is present on the surface of the calcined catalyst precursor. It should be noted that the cobalt oxide surface phase may contain some Co^{3+} as well as Co^{2+}, as concluded by Arnoldy and Moulijin [12] and Okamoto et al. [27]. The low temperature shoulder of the TPR peak (indicated by the arrow in Fig. 2) of the Co-HTC precursor supports this statement; here Co^{3+} present in the surface phase could be reduced to Co^{2+}.

Upon passivation a new surface oxide species is formed, as becomes evident from the hydrogen consumption in region I in the TPR patterns. This consumption corresponds to the reduction of the oxide skin of the passivated nickel and cobalt clusters on the surface. Similar observations were reported by Vos et al. [15] for nickel and for cobalt by Enache et al. [28] who used a rather unorthodox passivation procedure by exposing the reduced catalyst directly to air.

4.2. Characterization of the metal nanoparticles

By combining hydrogen chemisorption and TPR the dispersion and metal particle size of the nickel and cobalt clusters could be calculated. For nickel the particle sizes are in excellent agreement with the HREM results (Table 4). Lindfors and Smeds [8] found smaller particle sizes on this type of catalyst, however with a lower nickel loading. For a comparable metal loading (15 wt% Ni) Bartholomew et al. [29] found larger particle sizes, but their catalyst was prepared using conventional techniques and a standard support (γ-Al_2O_3). The hydrogen chemisorption values for the cobalt catalyst are relatively low, which points to reduction problems in the chemisorption apparatus. The presence of water during the reduction step may be the cause of these problems. Zhang et al. [11] have shown that water vapor strongly inhibits the reduction process of supported cobalt oxides. Another cause may be that the passivated cobalt particles could require a higher temperature to fully reduce their oxide skin: Fig. 2 indicates that reduction starts around 523 K, which corresponds to the maximum temperature applied in the hydrogen chemisorption reduction procedure. Kaddouri and Mazzocchia [2] also reported very low dispersion values for several Co/Al_2O_3 and Co/SiO_2 catalysts, which they attributed to reduction issues. These results imply that the values found by hydrogen chemisorption for the cobalt catalyst probably do not agree with the actual metallic surface area, dispersion and particle size. Nevertheless, a correlation is observed between the dispersion data from hydrogen chemisorption and the metal/aluminum ratio from XPS (Table 4), indicating that the ranking of the hydrogen chemisorption values could still be indicative for dispersion. From the metal surface area obtained from the hydrogen chemisorption measurements and the hydrogen consumption measured by TPR, the oxygen content of the passivated surface species could be determined. For the nickel catalysts, an average of 2.0 ± 0.4 oxygen atoms per metal surface atom was found, in agreement with values previously reported for Ni/SiO_2 catalysts [14,17]. This might indicate that two nickel layers are oxidized upon passivation, however, this contradicts previously reported EXAFS results for this catalyst which indicate that only one layer is oxidized [7]. For the nickel catalysts this paradox may be explained by the presence of a large amount of chemisorbed oxygen, as was observed for the oxidic precursors as well. For cobalt however, a much higher value of 7.5 ± 1.0 oxygen atoms per metal surface atom was found. This high value is due to the experimental error in the hydrogen chemisorption data (*vide supra*). The oxidic fraction determined by XPS can also be interpreted as a measure for the thickness of the oxide skin of the metallic clusters, assuming this is the only species present on the surface. In this case the values for nickel and cobalt are quite similar (Table 3), indicating a comparable thickness of the oxide layer. Van 't Blik and Prins reported a value of three oxygen atoms per cobalt atom using TPR on a Co/γ-Al_2O_3 catalyst [30], and the valence of cobalt in this phase is mainly +2, as evidenced by Jongsomjit et al. using Raman spectroscopy [25]. Hence, it is concluded that the passivated catalysts contain approximately two oxygen atoms per surface Ni or Co atom.

4.3. Stability of the metal particles against sintering

By comparing the different pretreatment procedures it becomes clear that for nickel catalysts temperature plays a

crucial role, whereas for the cobalt catalyst time on stream appears to be more critical. This agrees with the results of Bartholomew et al. who showed that the major part of the nickel surface area was lost during the first hours on stream in hydrogen at high temperature [29]. As can be seen in Table 3, increasing the reduction temperature for the nickel catalyst from 873 to 1123 K leads to a substantial increase in particle size. Prolonging the treatment at 1123 K has very little effect. In contrast, for the cobalt catalyst this same treatment leads to major sintering. The cobalt nanoparticles exhibit a much lower sintering rate at high temperatures, shown by the fact that the cobalt catalyst reduced at 873 K for 4 h has a lower dispersion than the one treated at 1123 K during 1 h. For nickel, the situation is reversed. These conclusions indicate that the activation energy for sintering is significantly higher for nickel than for cobalt.

The TPR profiles (Figs. 1 and 2) show a clear difference between the cobalt and nickel nanoparticles. In the case of cobalt the reduction peak of the oxide skin (region I) shows significant tailing to the high or low temperature side. This indicates a skewed particle size distribution, or maybe even a bidisperse system as observed by Enache et al. [28], in which the smaller particles exhibit stronger metal–support interactions and therefore reduce at a slightly higher temperature than the larger particles. This may explain the odd peak shape of the cobalt catalyst reduced at 1123 K during 1 h. Apparently an active cobalt species of very small particles is formed with a relatively high stability at this temperature. Prolonged reduction at 1123 K results in sintering of these particles forming larger clusters with a lower support interaction. Indeed the peak maximum shifts to a lower temperature in the TPR pattern. This hypothesis was tested by counting and sizing the number of particles visible in the HREM micrographs of these two cobalt catalysts (Co1123/1 and Co1123/4). Because the TPR peak is proportional to the surface area of the oxide skin, the obtained particle size distribution was converted to a specific surface area distribution by multiplying the number of particles to the squared particle diameter. Fig. 5 shows the results: indeed the catalyst reduced for only 1 h shows a homogeneous distribution with an average of about 12 nm. After 4 h of reduction the catalyst shows a rather distorted distribution of which the average has shifted towards 22 nm, and is highly skewed towards larger particles. These results confirm the proposed theory that for the cobalt catalyst a short reduction treatment at high temperature forms small particles, which sinter during prolonged treatment. In contrast, high temperature reduction of the nickel catalyst results in large particles.

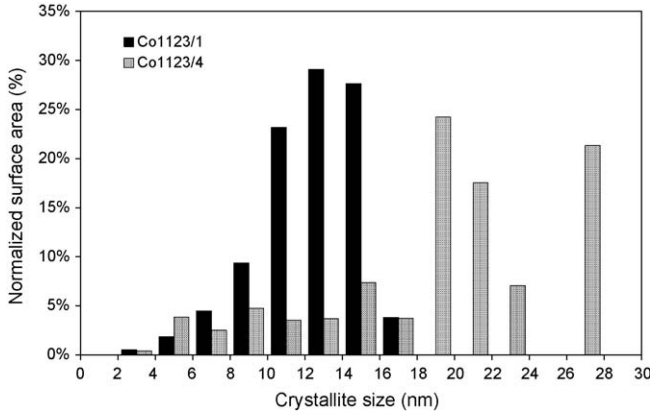

Fig. 5. Surface area distribution versus cobalt cluster size by HREM as function of reduction time at 1123 K.

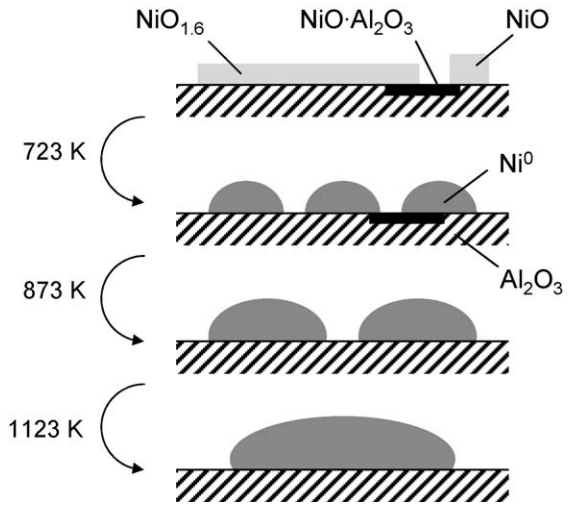

Fig. 6. Model for the reduction of the nickel catalyst.

4.4. Model of the catalyst before and after reduction

Figs. 6 and 7 show a schematic model of the reduction process of the nickel and cobalt based catalyst respectively. The oxidic precursors contain 3 phases; bulk NiO or Co_3O_4, a highly dispersed surface oxide and an aluminate like species. The surface phase was found to have a bulk formula of $NiO_{1.6}$ or $CoO_{1.6}$ in which nickel has a +2 valence and cobalt exists as Co^{2+} and possibly some Co^{3+}. Hence, a large amount of chemisorbed oxygen is present in these phases. Especially for the nickel catalyst, the predominant phase is the surface oxide, resulting in a homogeneous particle distribution with a very high dispersion upon reduction. After a short reduction time the active phase of the cobalt catalyst exhibits a less homogeneous particle size distribution; larger particles originated from the bulk Co_3O_4 crystallites and smaller particles from the highly dispersed cobalt oxide surface phase. After prolonged reduction the particle size distribution becomes highly distorted showing the clustering of small nanoparticles to form very large metallic particles.

The optimum reduction conditions can be defined using this model. On the one hand, the dispersion of the metallic clusters should be maximized (or their size minimized), yielding the

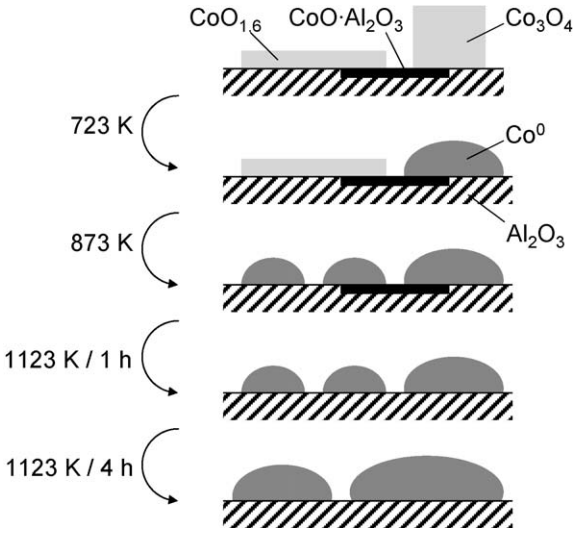

Fig. 7. Model for the reduction of the cobalt catalyst.

highest number of accessible sites on the metal surface. On the other hand, the reduction degree should be optimized, resulting in the maximum utilization of the metals available on the catalyst (given that non-reduced metal oxides are inactive), but at the cost of a reduced dispersion. Combining these factors, an optimum is reached at the maximum available metal surface area per gram of catalyst. Table 2 shows that the optimum reduction conditions found in this study are 873 K/4 h for the nickel catalyst, and 1123 K/1 h for the cobalt catalyst.

5. Conclusions

The oxidic precursors of the nickel and cobalt catalysts both contain a large amount of highly dispersed surface oxide, with a bulk formula of $NiO_{1.6}$ or $CoO_{1.6}$. These phases have a strong interaction with the support, contain a large amount of chemisorbed oxygen, and lead to the formation of highly dispersed nickel or cobalt nanoparticles upon reduction.

Upon passivation the outer layer of metal atoms is oxidized, containing approximately two oxygen atoms per surface Ni or Co atom. Passivated cobalt particles of smaller size appear to exhibit a stronger support interaction than larger particles, and reduce at slightly higher temperature.

Between nickel and cobalt pronounced differences were found for the reduction process and stability of the resulting metal nanoparticles. For nickel catalysts the reduction temperature plays a crucial role, whereas time is more critical for the cobalt catalyst. This indicates that the sintering rate of cobalt is considerably lower than that of nickel. It is concluded that the activation energy for sintering is significantly higher for nickel than for cobalt.

For the nickel catalyst, the optimal reduction conditions are around 823 K. Higher temperatures result in a lower metal surface area due to sintering. Reduction time was not found to be a major factor. For cobalt, the optimal conditions are around 1123 K and 1 h. Longer times cause major sintering, while at lower temperatures the catalyst is not completely reduced.

Acknowledgements

Johnson Matthey is gratefully acknowledged for financial support. Dr. B.W. Hoffer, Dr. E.J.M. Fakkeldij and Dr. J.C. Groen are gratefully acknowledged for their contributions to this work.

References

[1] I. Arslan, J.C. Walmsley, E. Rytter, E. Bergene, P.A. Midgley, J. Am. Chem. Soc. 130 (2008) 5716–5719.
[2] A. Kaddouri, C. Mazzocchia, Catal. Commun. 5 (2004) 339–345.
[3] E. Heracleous, A.F. Leeb, K. Wilson, A.A. Lemonidou, J. Catal. 231 (2005) 159–171.
[4] K.M. Hardiman, C.G. Cooper, A.A. Adesina, Ind. Eng. Chem. Res. 43 (2004) 6006–6013.
[5] Y. Zhang, Y. Zhang, C. Feng, C. Qiu, Y. Wen, J. Zhao, Catal. Commun. 10 (2009) 1454–1458.
[6] B.W. Hoffer, A.D. van Langeveld, J.P. Janssens, R.L.C. Bonné, C.M. Lok, J.A. Moulijn, J. Catal. 192 (2000) 432–440.
[7] T. Shido, M. Lok, R. Prins, Top. Catal. 8 (1999) 223–236.
[8] L.P. Lindfors, S. Smeds, Catal. Lett. 28 (1994) 291–299.
[9] P. Arnoldy, J.L. de Booys, B. Scheffer, J.A. Moulijn, J. Catal. 96 (1985) 122–138.
[10] Y. Okamoto, K. Nagata, T. Adachi, T. Imanaka, K. Inamura, T. Takyu, J. Phys. Chem. 95 (1991) 310–319.
[11] Y.L. Zhang, D.G. Wei, S. Hammache, J.G. Goodwin, J. Catal. 188 (1999) 281–290.
[12] P. Arnoldy, J.A. Moulijn, J. Catal. 93 (1985) 38–54.
[13] F.P.J.M. Kerkhof, J.A. Moulijn, J. Phys. Chem. 83 (1979) 1612–1619.
[14] J.W.E. Coenen, B.G. Linsen, Physical and Chemical Aspects of Adsorbents and Catalysts, Academic Press, London/New York, 1970, pp. 472–572.
[15] B. Vos, E. Poels, A. Bliek, J. Catal. 198 (2001) 77–88.
[16] M. Lo Jacono, M. Schiavello, A. Cimino, J. Phys. Chem. 75 (1971) 1044–1050.
[17] B. Mile, D. Stirling, M.A. Zammitt, A. Lovell, M. Webb, J. Catal. 114 (1988) 217–229.
[18] O. Clause, B. Rebours, E. Merlen, F. Trifiro, A. Vaccari, J. Catal. 133 (1992) 231–246.
[19] M. Houalla, J. Lemaitre, B. Delmon, J. Chem. Soc.: Faraday Trans. 78 (1982) 1389–1400.
[20] L. Ji, J. Lin, H.C. Zeng, J. Phys. Chem. B 104 (2000) 1783–1790.
[21] B. Scheffer, P. Molhoek, J.A. Moulijn, Appl. Catal. 46 (1989) 11–30.
[22] C.L. Bianchi, Catal. Lett. 76 (2001) 155–159.
[23] A. Lapidus, A. Krylova, V. Kazanskii, V. Borovkov, A. Zaitsev, J. Rathousky, A. Zukal, M. Jancalkova, Appl. Catal. 73 (1991) 65–82.
[24] W.J. Wang, Y.W. Chen, Appl. Catal. 77 (1991) 223–233.
[25] B. Jongsomjit, J. Panpranot, J.G. Goodwin, J. Catal. 204 (2001) 98–109.
[26] A. Kogelbauer, J.G. Goodwin, R. Oukaci, J. Catal. 160 (1996) 125–133.
[27] Y. Okamoto, T. Adachi, K. Nagata, M. Odawara, T. Imanaka, Appl. Catal. 73 (1991) 249–265.
[28] D.I. Enache, B. Rebours, M. Roy-Auberger, R. Revel, J. Catal. 205 (2002) 346–353.
[29] C.H. Bartholomew, R.B. Pannell, R.W. Fowler, J. Catal. 79 (1983) 34–46.
[30] H.F.J. Van 't Blik, R. Prins, J. Catal. 97 (1986) 188–199.